Article

Assessment of Electron Transfer Mechanisms during a Long-Term Sediment Microbial Fuel Cell Operation

Luciana Peixoto [1], Pier Parpot [1,2] and Gilberto Martins [1,*]

[1] Centre of Biological Engineering, University of Minho, Campus de Gualtar, 4710-057 Braga, Portugal; luciana.peixoto@deb.uminho.pt (L.P.); parpot@quimica.uminho.pt (P.P.)

[2] Centre of Chemistry, University of Minho, Campus de Gualtar, 4710-057 Braga, Portugal

* Correspondence: gilberto.martins@deb.uminho.pt; Tel.: +351-253604412

check for updates

Abstract: The decentralized production of bioelectricity as well as the bioremediation of contaminated sediments might be achieved by the incorporation of an anode into anaerobic sediments and a cathode suspended in the water column. In this context, a sediment microbial fuel cell microcosm was carried out using different configurations of electrodes and types of materials (carbon and stainless steel). The results showed a long-term continuous production of electricity (>300 days), with a maximum voltage of approximately 100 mV reached after ~30 days of operation. A twofold increase of voltage was noticed with a twofold increase of surface area (~30 mV to ~60 mV vs. 40 cm^2 to 80 cm^2), while a threefold increase was obtained after the substitution of a carbon anode by one of stainless steel (~20 mV to ~65 mV vs. 40 cm^2 to 812 cm^2). Cyclic voltammetry was used to evaluate sediment bacteria electroactivity and to determine the kinetic parameters of redox reactions. The voltammetric results showed that redox processes were limited by the diffusion step and corresponded to a quasi-reversible electron charge transfer. These results are encouraging and give important information for the further optimization of sediment microbial fuel cell performance towards the long-term operation of sediment microbial fuel cell devices.

Keywords: bioelectricity; sediment microbial fuel cell; cyclic voltammetry; long-term assessment

1. Introduction

Electricity can be gathered from aquatic sediments (both freshwater and marine sediments) by electroactive microorganisms growing on the surface of an anode [1,2]. Microorganisms in sediments mediate several processes in the biogeochemical cycles of carbon, nitrogen, phosphorus, metals, and sulphur [3], playing an important role in the dynamics and quality of aquatic ecosystems. Thus, a rational and integrated management of contaminated sediments is required [4]. The interaction with sediments can be engineered to provide artificial bioservices. One bioservice is the Sediment Microbial Fuel Cell (SMFC) that consists of an anode buried in the anoxic sediment and a cathode suspended in the aerobic water column connected by an external resistor [5,6]. Bacteria in a SMFC mediate the transfer of electrons from carbon sources to the anode, thus generating an electric current. SMFCs can provide continuous low-level power and do not require maintenance or replacement since power generation is not limited by the fuel supply; sediment organic matter is renewable (for example, new organic matter arrives to the sediments through the sedimentation of dead algae) and the electrodes of SMFCs are inert materials [6–8].

Currently, the main application described in the literature for SMFCs is as a long-term power source for autonomous sensors and communication devices [8]. In addition, SMFCs have also been explored as one type of new technology for removing organic matter from sediments [5,9,10] and for controlling phosphorus solubilization in eutrophic lake sediments [11–13].

Nevertheless, due to various limiting factors such as substrate mass transfer limitations and low electric conductivity, especially in freshwater, internal resistances in SMFCs are, generally, higher than those in microbial fuel cell (MFC) chambers [14,15]. This fact results in lower voltage and power output from SMFCs, with the typical reported values for power density, both for marine water and freshwater, varying from 0.18 to 81 mW·m^{-2} [5,16,17]. Moreover, several attempts have been made to improve SMFC performance through optimizing external resistance [10], improving sediment conductivity [18], using colloidal iron oxyhydroxide amendment [14], modifying electrode materials [19–23], and changing electrode configurations and assembly [24,25]. In addition, the amendment of sediments with new organic matter, such as glucose, plant rhizodeposits, or biomass like chitin or cellulose can also increase power production [15,26]. However, few studies have focused on the optimization of anodic material and structure.

Power generation in SMFCs also depends on the extracellular electron flow towards the anode created by electrogenic bacteria during the oxidation of organic matter. Nevertheless, and contrary to microbial fuel cell studies where indirect and direct electron transfer mechanisms of exoelectrogens and electrotrophs are well investigated, in SMFCs the electron transfer mechanisms are not well known [6].

Therefore, in order to optimize the bioelectricity production process from benthic systems, the goal of the present study was to assess the electron transfer mechanisms during a long term SMFC operation. For that, a SMFC microcosm was constructed and changes to electrodes configuration and materials were promoted.

2. Materials and Methods

2.1. Sediment Sampling

The sediments were collected at Lake Furnas (Azores, Portugal) with a gravitational Uwitec-corer that penetrated about 30 cm in the soft sediments. The sediments were immediately transported to the laboratory (at 4 °C), where the upper 10 cm layer was sliced, mixed, and stored frozen until usage. Sediments from Lake Furnas have a close relation with pumice deposits resulted from ancient volcano eruptions, with the granulometric analysis showing a finer fraction composed by silt and clay. These sediments had 78% ± 1% water content and 10% ± 1% organic matter content. More properties of the sediments and water column of Lake Furnas can be found in Martins et al. [27].

2.2. Sediment Microbial Fuel Cell Start-up and Operation

A sediment microbial fuel cell (SMFC) microcosm was set-up to assess the electroactivity of sediment bacteria (Figure 1). In brief, a 1 L open reactor was filled with ~400 g of sediment and 500 mL of tap water. The anode was buried in the sediments (between 3 cm and 4 cm depth) and the cathode was submerged in the water (±1 cm above the water–sediment interface). Figure 1 shows the experimental set-up used in the present work. As electrode material, two types of materials were used: carbon Toray (4 cm × 5 cm), with proven capabilities to work as a SMFC anode [16], and a low cost stainless steel scourer (Scotch-Brite, 3M, St. Paul, MN, USA), easily found in a grocery store. The electrodes were connected via a 1000 Ω resistor during the first 33 days and via a 2000 Ω resistor thereafter. The voltage was recorded by a USB-9215A BNC connector datalogger (National Instruments, Austin, TX, USA) and data acquisition software (Labview 6.0, National Instruments, Austin, TX, USA). Different configurations of electrodes were tested according to Table 1.
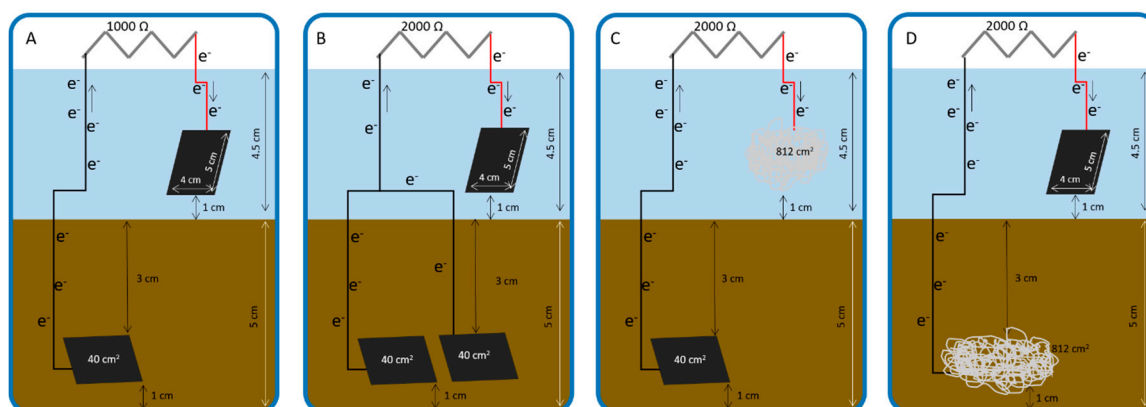
Figure 1. Sediment Microbial Fuel Cell (SMFC) experimental set-up; (**A**) one carbon Toray anode and one carbon Toray cathode; (**B**) two carbon Toray anodes and one carbon Toray cathode; (**C**) one carbon Toray anode and one stainless steel scourer cathode; and (**D**) one stainless steel scourer anode and one carbon Toray cathode.

Table 1. Summary of electrode materials and configurations tested during the assay.

Operation Day	Anode Material	Anode Area/cm^2	Cathode Material	Cathode Area/cm^2	External Resistor/Ω
1	carbon Toray	40	carbon Toray	40	1000
33 (a)	carbon Toray	40	carbon Toray	40	2000
88 (b)	carbon Toray	80 *	carbon Toray	40	2000
185 (c)	carbon Toray	80 *	stainless steel	812	2000
206 [#] (d)	carbon Toray	40	stainless steel	812	2000
286 [$] (e)	stainless steel	812	carbon Toray	40	2000

(a), (b), (c), (d), (e) correspond to the points indicated in Figure 2. * two carbon Toray electrodes in parallel with 40 cm^2 each. [#] addition of acetate to the water column. [$] change of electrodes (the anode was placed in the water column and the cathode was embedded in the sediments).

Current intensity (*I*) was calculated following the Ohm´s law, and the current density (*j*) was calculated as $j = I/A$, where A is the projected surface area of the anode electrode. The power density (*P*) was calculated as the product of current intensity and voltage (*V*) divided by the surface area of the anode ($P = IV/A$). For the polarization curve determination, the anode and cathode in the SMFC were connected to a resistance box and the voltage was recorded for a series of resistances between 41 kΩ to 50 Ω. The internal resistance of the SMFC (*Rint*) was calculated from the slope of the polarization curve in the region dominated by Ohmic losses [16]. The open circuit voltage (*OCV*) was measured at infinite resistance.

2.3. Cyclic Voltammetry

The oxidation–reduction reactions at the surface of a working electrode (anode) was characterized by cyclic voltammetry at day 35 of SMFC operation for the carbon Toray anode and at day 310 for stainless steel anode. This was intended to guarantee that both electrodes spent a similar time embedded in sediments and had a stable current density production. The SMFC was used as an electrochemical cell. The working electrode was the anode buried in sediments, the counter electrode was the cathode submerged in the water column, and the reference electrode, a Saturated Calomel Electrode (SCE), was situated near to the working electrode. The electrodes were connected to a potentiostat (Model 2051, Amel Instruments, Milan, Italy). The response of current intensity (*I*) to the potential (*E*), in an interval from −850 mV to 900 mV vs. SCE, was recorded directly from the potentiostat output at a scan rate of 50 mV·s^{-1}. A LabVIEW-based acquisition system via a universal serial bus interface (USB, Intel, Santa Clara, CA, USA) was used to record the obtained data. The kinetic parameters of the redox processes associated to oxidation peaks observed in cyclic voltammograms

obtained at 50 mV·s^{-1} were assessed by running different cyclic voltametries with different scan rates (from 5 mV·s^{-1} to 1000 mV·s^{-1}). The reversibility of the electronic transfer was calculated by analyzing the dependence of the peak potential on the scan rate; when a peak potential is dependent on scan rate, it indicates an irreversible process, and when the peak potential is independent on scan rate, it indicates a reversible process [28]. Also, the linearity of the Randles−Sevcik equation was evaluated.

2.4. Principal Component Analysis (PCA)

The multivariate statistical method PCA was used to examine relationships in a data set. The PCA method was implemented according to Gabriel [29] and Martins et al. [27]. Eigenvalues and eigenvectors were extracted from the covariance matrix of the original variables to illustrate associations among variables that otherwise might be hidden. The complete dataset used in this study was a two-way table of six columns with the variables anode area, maximum voltage (max *V*), *OCV*, maximum current density (max *j*), maximum power density (max *P*), and internal resistance (*Rint*) and three rows with the observations obtained for the SMFC configuration with only one carbon Toray anode, two carbon Toray anodes, and one stainless steel anode. All mathematical and statistical computations were made using XLSTAT 2019.1.1.56159 (Addinsoft, Paris, France).

3. Results

3.1. Sediment Microbial Fuel Cell Microcosm

The voltage was measured along the operation time of the SMFC assay and is depicted in Figure 2. The results showed a continuous production of bioelectricity for a long period (~200 days) without the addition of external sources of organic matter (Figure 2).
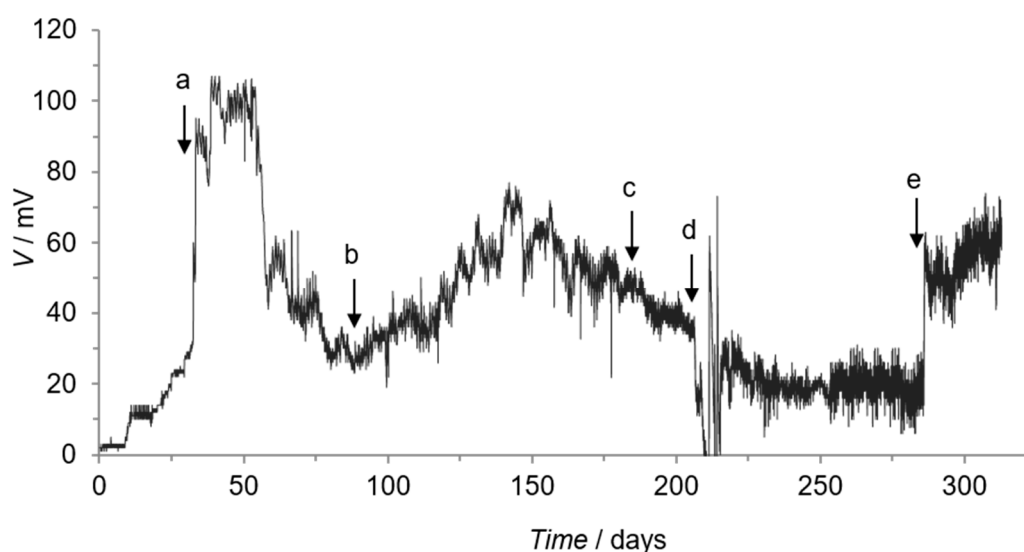

Figure 2. Variation of voltage over SMFC operation; (a) change of external resistance; (b) introduction of new carbon Toray anode in sediments; (c) cathode switch from carbon Toray to stainless steel electrode; (d) addition of acetate in the water column; (e) switch of electrodes, the cathode was introduced in the sediments (as a new anode) and the anode was placed in the water column (in order to be used as a new cathode).

The voltage increased during the first 40 days of SMFC operation, reaching a maximum voltage around 100 mV (Figure 2). Afterwards, voltage started to decrease to around 30 mV. This decrease was probably due to the depletion of easily biodegradable compounds in the sediment around the anode. After the introduction of a new anode (of the same material and with a similar surface area) in the sediments (b), voltage rose again, reaching values around 70 mV. On the other hand, the addition

of acetate (d) as a new carbon source did not result in an increase of voltage, but rather a decrease. This result was probably due to the increase of oxygen consumption rate in the water column, which might limit the availability of oxygen to serve as a terminal electron acceptor [30]. The replacement of a carbon Toray cathode to stainless steel cathode (c) did not result in an effective change in voltage, since voltage maintained the same trend of decay. The voltage only started increasing again (until ~65 mV) when both electrodes in the SMFC were switched (i.e., the stainless steel electrode was introduced in the sediments and the carbon Toray electrode was placed in the water column).

Regarding current density, the external resistance changed and the introduction of a stainless steel electrode with a higher surface area resulted in a decrease of current density values. Also, power density values were very low during all experiments, with the maximum value (1.42 mW·m^{-2}) reached at day 40.

During the stable phase of power generation, polarization and power curves were obtained by varying the external resistance from 71 kΩ to 50 Ω (Figure 3). Current densities varied between 0.042 ± 0.003 mA·m^{-2} for the stainless steel scourer anode and 18.75 ± 1.41 mA·m^{-2} for the carbon Toray anode. The *OCV* was higher for the SMFC with one carbon Toray anode and cathode (352 ± 2.64 mV) than for the configuration with two carbon Toray anodes in parallel and a stainless steel scourer cathode (157 ± 1.18 mV). The SMFC *OCV* with the stainless steel scourer anode and carbon Toray cathode was 254 ± 1.91 mV.
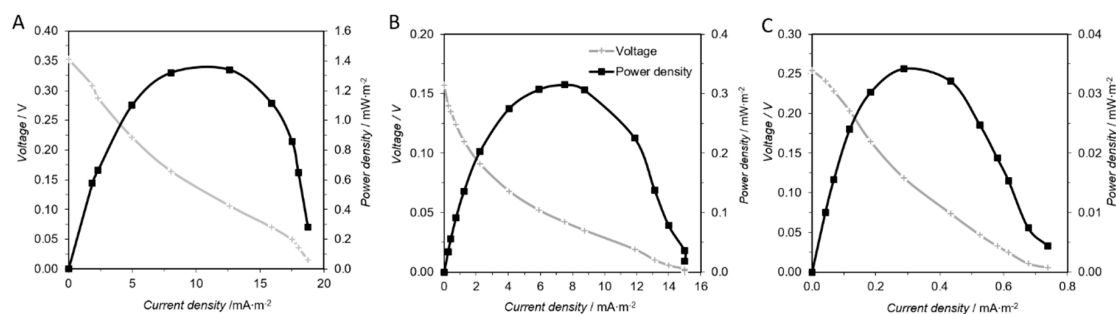

Figure 3. Power and polarization curves obtained during SMFC operation with (**A**) a carbon Toray anode and cathode (determined at day 34); (**B**) SFMC with two carbon Toray anodes and a stainless steel scourer cathode (determined at day 130); and (**C**) SMFC with stainless steel scourer anode and a carbon Toray cathode (determined at day 310).

In the case of only one carbon Toray anode, the maximum power density was similar to the maximum power density obtained in the microcosm (~1.4 ± 0.11 mW·m^{-2}). For the other configurations, the values were considerably lower (0.32 ± 0.024 mW·m^{-2} in the situation of two carbon Toray anodes, and 0.03 ± 0.002 mW·m^{-2} for the stainless steel scourer anode and a carbon Toray cathode). Moreover, the shape of the polarization curves suggested high activation losses on the SMFC configuration with two carbon Toray anodes. For the other two configurations, the polarization curves did not show this initial sharp decrease of voltage for low current densities. The results of the polarization curve also indicate that the optimum resistance, i.e., the resistance for which the maximum power density was obtained, was around 2100 Ω for the situation with only one carbon anode and 700 Ω for the configuration with the two carbon anodes. For the SMFC with a stainless steel scourer anode, the best resistor was around 5000 Ω. Based on the slope of the polarization curve in the area dominated by ohmic losses, it was observed that the internal resistance of the system with the stainless steel anode (2374 ± 178 Ω) and carbon cathode was much higher than the internal resistance of the systems with a carbon anode (120 ± 9 Ω) and two carbon anodes (55 ± 4 Ω).

3.2. Cyclic Voltammetry Assessments

Cyclic voltammetric experiments were carried out at 50 mV·s^{-1} with the different anode configurations tested in the SMFC microcosms. Figure 4 presents the cyclic voltammograms of carbon Toray and stainless steel as working electrodes in the microcosm environment (i.e., the working and reference electrodes inserted in sediments, the counter electrode submerged in the water column.
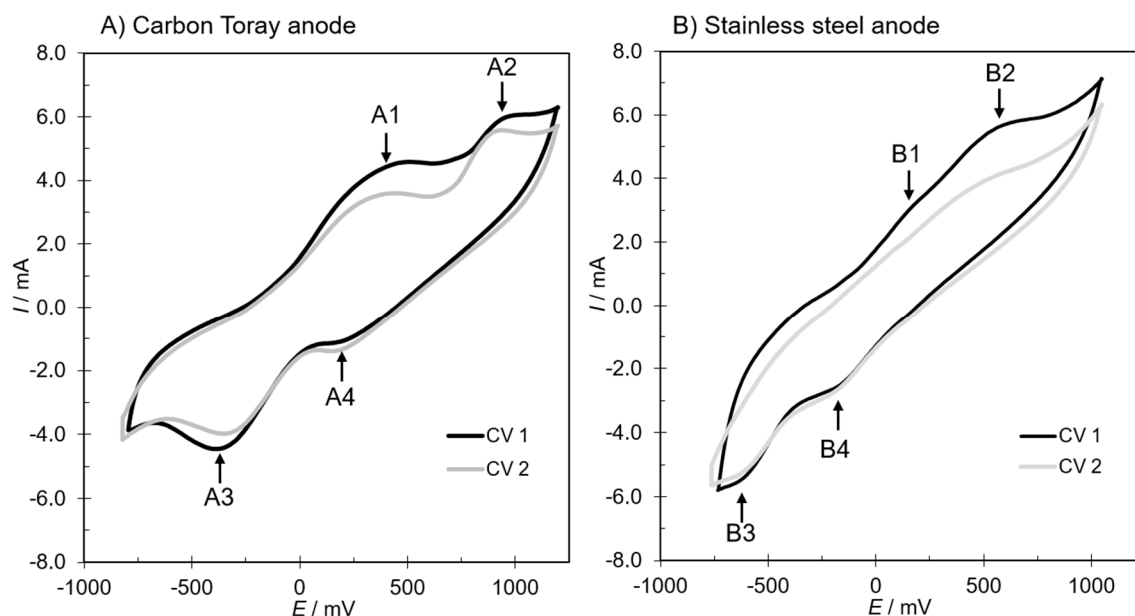
Figure 4. Cyclic voltammograms of carbon Toray (**A**) and stainless steel (**B**) in the SMFC recorded at 50 mV·s^{-1}.

In the voltammograms of carbon Toray and stainless steel anodes it is possible to observe an increase of the overall current intensities for the potential region between -0.50 V and 0.95 V vs. SCE. With carbon Toray, two oxidation peaks were observed during the positive sweep at 0.435 V (peak A1) and 0.960 V (peak A2) vs. SCE, and two reduction peaks were observed during the negative sweep at -0.370 V (peak A3) and 0.203 V (peak A4) vs. SCE, respectively. The corresponding current intensities for the peaks A1, A2, A3, and A4 were, respectively, 4.05 ± 0.35 mA, 5.77 ± 0.21 mA, -4.21 ± 0.24 mA, and -1.20 ± 0.13 mA (Figure 4A). The stainless steel anode exhibited an oxidation wave between 0.18 V and 0.86 V vs. SCE with two moderate current intensities highlighted at 0.185 V and 0.60 V vs. SCE with 2.77 ± 0.45 mA and 4.95 ± 0.75 mA, respectively (Peak B1 and B2), which can be attributed to the successive oxidation processes, suggesting that the different redox species present in the sediments contributed to the current intensities. In the reverse scan, two reduction peaks were observed at -0.620 V and -0.248 V vs. SCE with -5.34 ± 0.10 mA and -2.85 ± 0.08 mA, respectively (Peak B3 and B4). In both voltammograms the redox reactions appear to be quasi-reversible behavior. The global shape of the voltammograms also reveals a high internal resistance, which was already expected since the anodes were not in aqueous solution but introduced in sediments with low ionic conductivity.

The kinetic study of the oxidation peaks (A1, A2, B1, and B2) assessed by cyclic voltammetry at different sweep scan rates (from 5 mV·s^{-1} to 1000 mV·s^{-1}) are depicted in Figures 5 and 6.
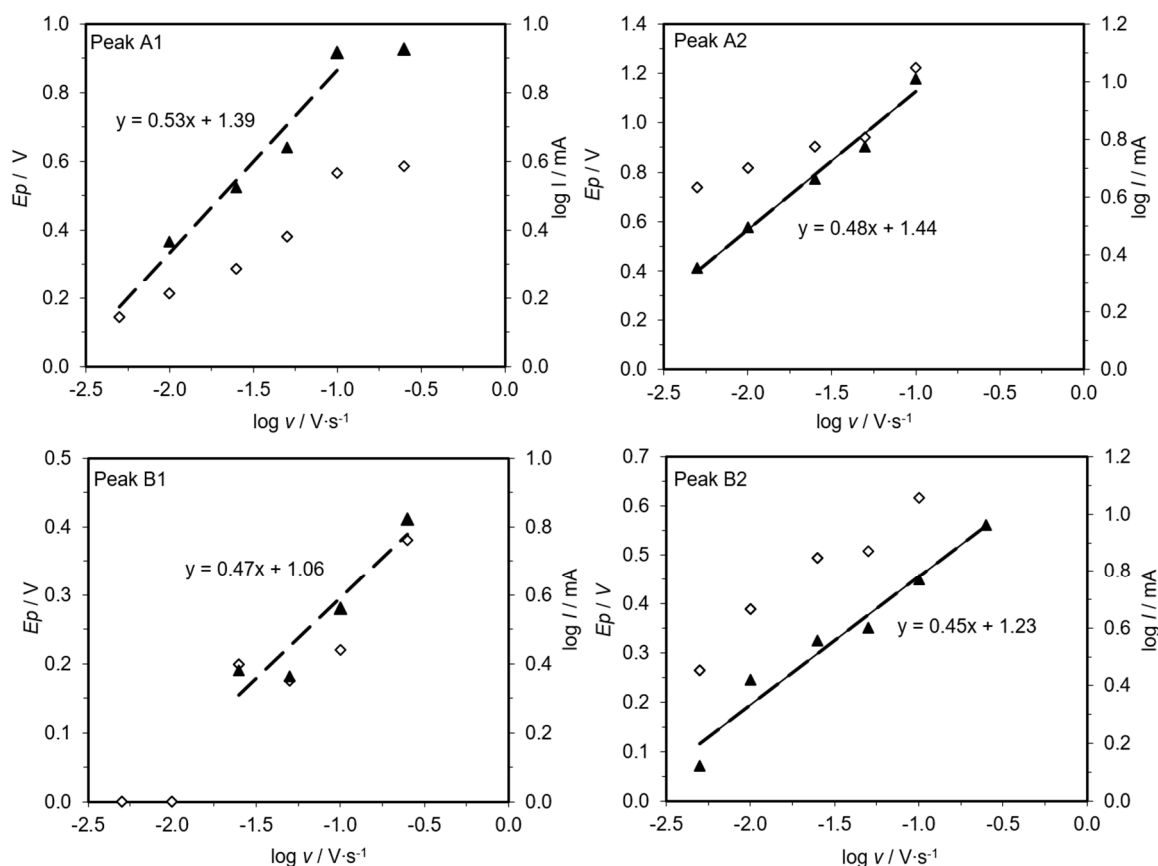
Figure 5. The log (I/mA) vs. log (v/V·s^{-1}) (▲) and Ep vs. log (v/V·s^{-1}) (◇) curves for the distinguished oxidation peaks in the SMFC with the carbon Toray anode (peak A1 and peak A2) and with the stainless steel anode (peak B1 and peak B2).

Using carbon Toray as the SMFC anode, the slope value of the log I vs. log v curves in the entire scan rate region for peaks A1 and A2 were, respectively, 0.53 and 0.48. The change of anodes did not promote significant changes in current density. For both peaks A1 and A2, the relation between E and log v (Figure 5) showed that the peak potential was dependent of the sweep rate, revealing an irreversible electron charge transfer [28]. Similar results were obtained with the stainless steel anode (peaks B1 and B2). However, as was mentioned before, the peaks were not well defined. Nevertheless, it was possible to observe more defined peaks at lower scan rates, corresponding to irreversible processes, where the diffusion is the main limitation step of the electron transfer (Figure 6). Furthermore, the results obtained with the kinetic study, namely the quasi-reversibility of the electron charge process, were in agreement with the expected results corresponding to the shape of the voltammograms at 50 mV·s^{-1}. In addition, Figure 6 shows that the Randles−Sevcik equation was not linear for all scan rates. This fact indicates the quasi-reversibility of the electrochemical processes, suggesting that in the SMFC the electron transfer mechanisms could be controlled by diffusional species [31].
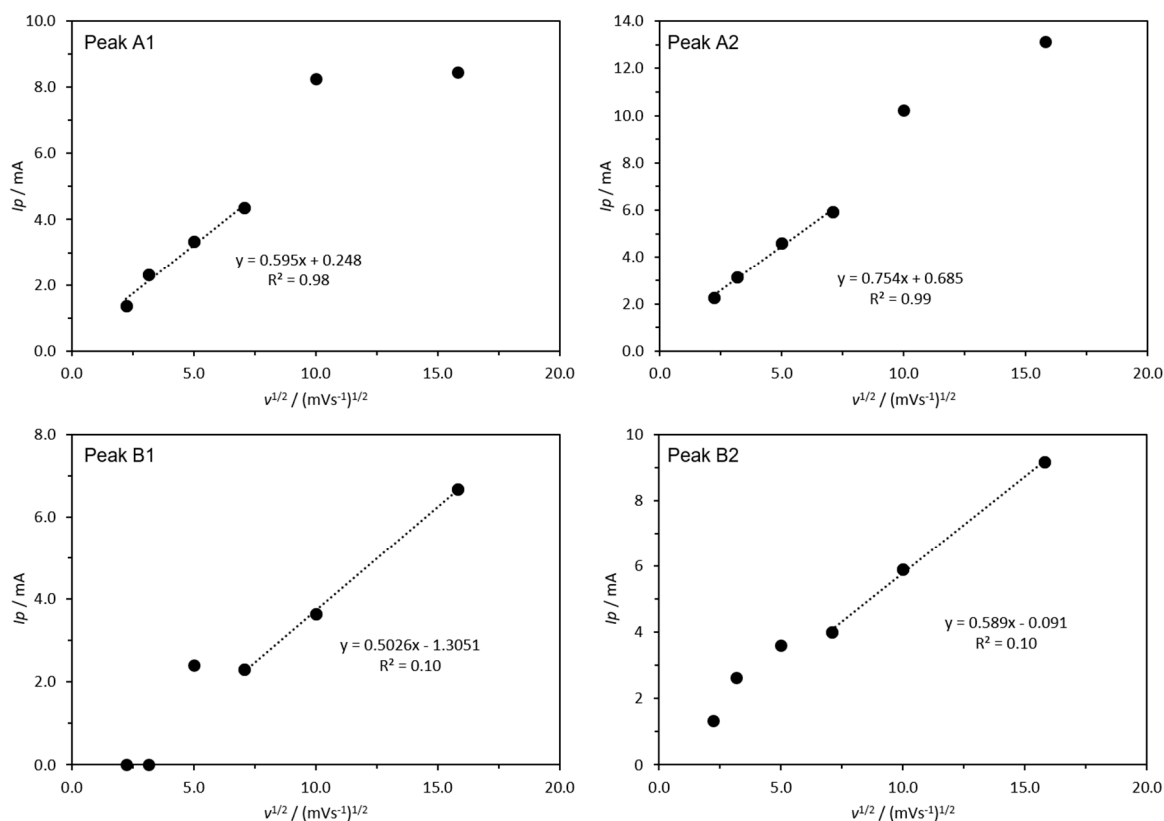
Figure 6. Curves of peak current intensity *Ip* vs. square root of scan rate ($v^{1/2}$) for the distinguished oxidation peaks in the SMFC with the carbon Toray anode (peak A1 and peak A2) and with the stainless steel anode (peak B1 and peak B2).

3.3. Principle Component Analysis

To interpret the relationships between the different variables, a PCA analysis with extracted principal components (PCs) was conducted. Two PCs with eigenvalues >1 were retained and captured 100% of the input variance using three observations and six variables. A PCA biplot for PC1 vs. PC2 (Figure 7) demonstrated that the different electrochemical variables, drawn as vectors, occupy different regions of the plot and exhibit well-defined patterns. PC1 explained 70% of the total variance and had positive loadings for all variables except for internal resistance and anode area. PC2 explained the other 30% of the original variability and had negative loadings only on maximum power density. Another important observation is that the three observations for the different anode configurations are spread in the plot of the PCA analysis, confirming that the obtained values did not have correlation between each other. The carbon Toray configuration clustered closer to the maximum power density, while the configuration with two carbon Toray anodes did not cluster with any variable. The stainless steel configuration clustered with the area of the electrode and with the internal resistance. This fact is in line with the observations made in Figures 2 and 3, where it was verified that the stainless steel configuration presented higher internal resistance.
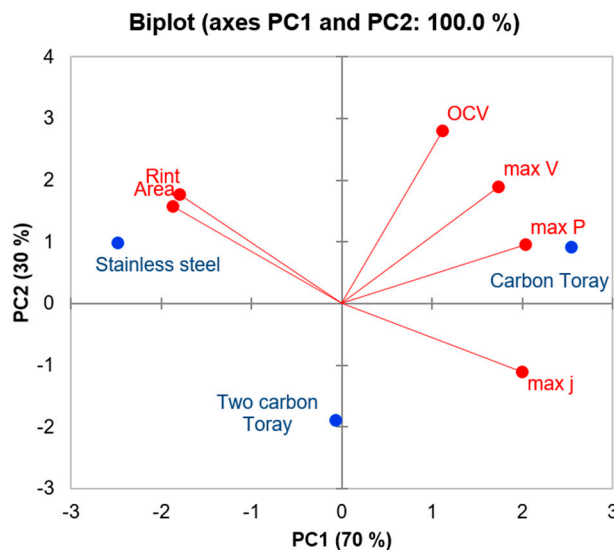
Figure 7. Principle component analysis (PCA) biplots of bioelectrochemical parameters.

4. Discussion

This work evaluated the bioelectroactivity of sediment bacteria and suggested that the primary routes involved in electron transfer were mainly indirect. This fact was verified by the slope (~0.5) of the log *I* vs. log *v* curves and the non-linearity of the Randles−Sevcik equation (Figures 5 and 6), which showed that the oxidation processes were mainly limited by diffusion [16,28]. In addition, no lag phases of electricity production were observed after the switch of the electrodes during the microcosm experiment (Figure 2). These achievements might indicate that sediment electroactive bacteria could prefer a mediated electron transfer over a direct electron transfer mechanism. In addition, Ewing et al. [21] also found that during a long-term SMFC operation, the presence or absence of an electroactive biofilm on the electrodes did not affect the power performance. However, Ryckelynck et al. [32] attributed the voltage generation without lag phases to the abiotic oxidation of inorganic electron donors at the anode. Also, Mitov et al. [33] showed that during long-term SMFC operation (i.e., after reaching a steady-state), the evaluated parameters (open circuit voltage, power density, current density, and internal resistance) tend to have high repeatability and reproducibility.

From this work, it is also important to note the high internal resistance of the stainless steel anode (almost 20× higher) compared to the internal resistance of the system with a carbon anode. Internal resistance is an important factor in SMFC performance, and its presence will undoubtedly consume part of the voltage and reduce the output power [20]. Besides, it appears that internal resistance was dependent on anode material and surface area, because in the present study, the different set-ups presented similar conditions of ionic strength and electrolyte pH (tap water as electrolyte and pH around 7.7) [34]. Another explanation for the higher internal resistance of the stainless steel anode could be the corrosion and passivation phenomena that might have occurred on the surface of the electrode. This phenomenon might have influenced the biofilm adhesion to the electrode material. In addition, a slow corrosion progress of the stainless steel anode was reported before [35]. However, the corrosion or other changes associated with stainless steel was also related to the improvement of cathode performance in a microbial electrolysis cell [36]. Thus, further research into stainless steel corrosion and its impacts on current generation in SMFCs is needed.

Furthermore, the variation of output power with the external resistance can be attributed to polarization losses (i.e., activation, ohmic, and concentration) across the SMFC [37]. Interestingly, in two of the four electrode configurations tested, the initial decrease of the slope of the polarization curves, usually due to activation losses, were not observed. This result might indicate that in those cases, the anodes already presented a mature biofilm or, more probably, a well-established route for electron transfer inside the sediments. For example, recent works have shown that cable bacteria can facilitate

the electron transfer from reduced to oxic zones both in marine and freshwater sediments [38–41]. In some cases, nitrate can substitute the oxygen and serve as the electron acceptor as well [42]. In addition, the tested electrode configurations that presented activation losses were the ones where the anodes spent less time buried in the sediments. Another explanation for the lower performance of the SMFC over time might be the cathodic reduction of oxygen. Asensio et al. [43] identified the cathodic reduction of oxygen as a bottleneck of the MFC performance with stainless steel electrodes and not with carbon felt.

Regarding the decreases of voltage over time, it might be attributed to mass transfer limitations, since all soluble organic carbon near the anode would be consumed [25,44], but also to the increase of internal resistance. Cathode biofouling, absence of bulk fluid velocity fluctuations, and mass transfer limitations may contribute to the increase of internal resistance [1,25,45]. It was also found that the improvements in current were temporary, indicating that the SMFCs need to be further optimized for long-term steady power performance [46]. Long-term operation studies are still scarce, but the data from these studies can be valuable for the development of renewable power sources for remote environmental monitoring [21].

The maximum power density obtained in the present work (1.4 mW·m^{-2}) was low when compared with the values found in the literature for similar setups. In freshwater environments, the maximum power densities observed for SMFCs with plane graphite disks [33], felt graphite [47], carbon paper [16], and granular activated carbon [35] as cathodes were 35.3 mW·m^{-2}, 4 mW·m^{-2}, 2 mW·m^{-2}, and 3.5 mW·m^{-2}, respectively, while a maximum power density from an SMFC with rotating Pt cathode [15] reached 49 mW·m^{-2}. Nevertheless, these values are all low when compared to value from MFCs using carbon felt as the anode and cathode: 1062 mW·m^{-2} [43]. Evidently, differences in maximum power densities can be explained not only in terms of the electrode materials but also because of the SMFC configurations, source, and type of inoculum, type and content of the organic matter present in sediments, and operation conditions.

Therefore, and due to the low amount of bioenergy recovery from these systems, we should also look for other potential applications of SMFCs. For example, it is well known that electroactive bacteria play an important role in the iron cycle [13]. In eutrophic lakes, the sediments have a high concentration of phosphorus bounded to iron oxides [48]. Thus, an SMFC might compete with the phosphorus dissolution process. By introducing the electrodes in sediments, we are creating a new route for the electrons. Martins et al. [25] already showed that in sediments impacted by the operation of a SMFC (along 50 days), the metal bound P fraction increased 3% and the organic P fraction decreased close to 10%. Another example of the application is the bioremediation of contaminated sediments by hydrocarbons [49]. For example, Bellagamba et al. [50] showed that the application of low-voltage electrolysis (2 V) accelerated (up to 3 times) the biodegradation of hydrocarbons from crude oil in marine sediments.

5. Conclusions

In conclusion, the increase of anode surface area resulted in an increase of bioelectricity production: a two-fold increase by duplicating the carbon Toray anode and a three-fold increase by substituting the carbon Toray anode by one of stainless steel. By contrast, the replacement of the carbon Toray cathode by the stainless steel cathode and the addition of acetate to the water column did not result in a significant change in the current density trend. The cyclic voltammetric results verified that the electron transfer process was mainly limited by diffusion, indicating the prevalence of indirect processes for electron transfer. Finally, MFC technology applied to benthic systems is presented as an interesting opportunity for ecosystem valorization, especially in eutrophic aquatic systems.

Author Contributions: L.P. and G.M. conceived the study, performed the experiments, and wrote the paper. P.P. participated in the discussions of the work and in the review and editing of the paper. All authors have approved the final version of the manuscript.

Conflicts of Interest: The authors declare no conflict of interest.

References

1. Tender, L.M.; Reimers, C.E.; Iii, H.A.S.; Holmes, D.E.; Bond, D.R.; Lowy, D.A.; Pilobello, K.; Fertig, S.J.; Lovley, D.R. Harnessing microbially generated power on the seafloor. *Nat. Biotechnol.* **2002**, *20*, 821–825. [CrossRef] [PubMed]

2. Holmes, D.E.; Bond, D.R.; O'Neil, R.A.; Reimers, C.E.; Tender, L.R.; Lovley, D.R. Microbial communities associated with electrodes harvesting electricity from a variety of aquatic sediments. *Microb. Ecol.* **2004**, *48*, 178–190. [CrossRef] [PubMed]

3. Martins, G.; Terada, A.; Ribeiro, D.C.; Corral, A.M.; Brito, A.G.; Smets, B.F.; Nogueira, R. Structure and activity of lacustrine sediment bacteria involved in nutrient and iron cycles. *FEMS Microbiol. Ecol.* **2011**, *77*, 666–679. [CrossRef] [PubMed]

4. Kwok, K.W.H.; Batley, G.E.; Wenning, R.J.; Zhu, L.; Vangheluwe, M.; Lee, S. Sediment quality guidelines: Challenges and opportunities for improving sediment management. *Environ. Sci. Pollut. Res.* **2014**, *21*, 17–27. [CrossRef] [PubMed]

5. Li, H.; Tian, Y.; Qu, Y.; Qiu, Y.; Liu, J.; Feng, Y. A Pilot-scale Benthic Microbial Electrochemical System (BMES) for Enhanced Organic Removal in Sediment Restoration. *Sci. Rep.* **2017**, *7*, 39802. [CrossRef] [PubMed]

6. Abbas, S.Z.; Rafatullah, M.; Ismail, N.; Syakir, M.I. A review on sediment microbial fuel cells as a new source of sustainable energy and heavy metal remediation: Mechanisms and future prospective. *Int. J. Energy Res.* **2017**, *41*, 1242–1264. [CrossRef]

7. Tender, L.M.; Gray, S.A.; Groveman, E.; Lowy, D.A.; Kauffman, P.; Melhado, J.; Tyce, R.C.; Flynn, D.; Petrecca, R.; Dobarro, J. The first demonstration of a microbial fuel cell as a viable power supply: Powering a meteorological buoy. *J. Power Sources* **2008**, *179*, 571–575. [CrossRef]

8. Donovan, C.; Dewan, A.; Heo, D.; Lewandowski, Z.; Beyenal, H. Sediment microbial fuel cell powering a submersible ultrasonic receiver: New approach to remote monitoring. *J. Power Sources* **2013**, *233*, 79–85. [CrossRef]

9. Song, N.; Jiang, H.L. Effects of initial sediment properties on start-up times for sediment microbial fuel cells. *Int. J. Hydrogen Energy* **2018**, *43*, 10082–10093. [CrossRef]

10. Song, T.-S.; Yan, Z.-S.; Zhao, Z.-W.; Jiang, H.-L. Removal of organic matter in freshwater sediment by microbial fuel cells at various external resistances. *J. Chem. Technol. Biotechnol.* **2010**, *85*, 1489–1493. [CrossRef]

11. Xu, P.; Xiao, E.; Xu, D.; Li, J.; Zhang, Y.; Dai, Z.; Zhou, Q.; Wu, Z. Enhanced phosphorus reduction in simulated eutrophic water: A comparative study of submerged macrophytes, sediment microbial fuel cells, and their combination. *Environ. Technol.* **2018**, *39*, 1144–1157. [CrossRef] [PubMed]

12. Yang, Q.; Zhao, H.; Zhao, N.; Ni, J.; Gu, X. Enhanced phosphorus flux from overlying water to sediment in a bioelectrochemical system. *Bioresour. Technol.* **2016**, *216*, 182–187. [CrossRef] [PubMed]

13. Martins, G.; Peixoto, L.; Brito, A.G.; Nogueira, R. Phosphorus-iron interaction in sediments: Can an electrode minimize phosphorus release from sediments? *Rev. Environ. Sci. Biotechnol.* **2014**, *13*, 265–275. [CrossRef]

14. Zhou, Y.-L.; Yang, Y.; Chen, M.; Zhao, Z.-W.; Jiang, H.-L. To improve the performance of sediment microbial fuel cell through amending colloidal iron oxyhydroxide into freshwater sediments. *Bioresour. Technol.* **2014**, *159*, 232–239. [CrossRef] [PubMed]

15. He, Z.; Shao, H.; Angenent, L.T. Increased power production from a sediment microbial fuel cell with a rotating cathode. *Biosens. Bioelectron.* **2007**, *22*, 3252–3255. [CrossRef] [PubMed]

16. Martins, G.; Peixoto, L.; Ribeiro, D.C.; Parpot, P.; Brito, A.G.; Nogueira, R. Towards implementation of a benthic microbial fuel cell in lake Furnas (Azores): Phylogenetic affiliation and electrochemical activity of sediment bacteria. *Bioelectrochemistry* **2010**, *78*, 67–71. [CrossRef] [PubMed]

17. Song, T.; Tan, W.; Wu, X.; Zhou, C.C. Effect of graphite felt and activated carbon fiber felt on performance of freshwater sediment microbial fuel cell. *J. Chem. Technol. Biotechnol.* **2012**, *87*, 1436–1440. [CrossRef]

18. Lenin Babu, M.; Venkata Mohan, S. Influence of graphite flake addition to sediment on electrogenesis in a sediment-type fuel cell. *Bioresour. Technol.* **2012**, *110*, 206–213. [CrossRef]

19. Sonawane, J.M.; Patil, S.A.; Ghosh, P.C.; Adeloju, S.B. Low-cost stainless-steel wool anodes modified with polyaniline and polypyrrole for high-performance microbial fuel cells. *J. Power Sources* **2018**, *379*, 103–114. [CrossRef]

20. Chen, W.; Liu, Z.; Su, G.; Fu, Y.; Zai, X.; Zhou, C.; Wang, J. Composite-modified anode by MnO_2/polypyrrole in marine benthic microbial fuel cells and its electrochemical performance. *Int. J. Energy Res.* **2017**, *41*, 845–853. [CrossRef]

21. Ewing, T.; Ha, P.T.; Beyenal, H. Evaluation of long-term performance of sediment microbial fuel cells and the role of natural resources. *Appl. Energy* **2017**, *192*, 490–497. [CrossRef]

22. Fu, Y.B.; Liu, Z.H.; Su, G.; Zai, X.R.; Ying, M.; Yu, J. Modified Carbon Anode by MWCNTs/PANI Used in Marine Sediment Microbial Fuel Cell and its Electrochemical Performance. *Fuel Cells* **2016**, *16*, 377–383. [CrossRef]

23. Fu, Y.; Xu, Q.; Zai, X.; Liu, Y.; Lu, Z. Low electrical potential anode modified with Fe/ferric oxide and its application in marine benthic microbial fuel cell with higher voltage and power output. *Appl. Surf. Sci.* **2014**, *289*, 472–477. [CrossRef]

24. An, J.; Kim, B.; Nam, J.; Ng, H.Y.; Chang, I.S. Comparison in performance of sediment microbial fuel cells according to depth of embedded anode. *Bioresour. Technol.* **2013**, *127*, 138–142. [CrossRef] [PubMed]

25. Martins, G.; Peixoto, L.; Teodorescu, S.; Parpot, P.; Nogueira, R.; Brito, A.G. Impact of an external electron acceptor on phosphorus mobility between water and sediments. *Bioresour. Technol.* **2014**, *151*, 419–423. [CrossRef] [PubMed]

26. De Schamphelaire, L.; Cabezas, A.; Marzorati, M.; Friedrich, M.W.; Boon, N.; Verstraete, W. Microbial community analysis of anodes from sediment microbial fuel cells powered by rhizodeposits of living rice plants. *Appl. Environ. Microbiol.* **2010**, *76*, 2002–2008. [CrossRef] [PubMed]

27. Martins, G.; Henriques, I.; Ribeiro, D.C.; Correia, A.; Bodelier, P.L.E.; Cruz, J.V.; Brito, A.G.; Nogueira, R. Bacterial Diversity and Geochemical Profiles in Sediments from Eutrophic Azorean Lakes. *Geomicrobiol. J.* **2012**, *29*, 704–715. [CrossRef]

28. Parpot, P.; Santos, P.R.B.; Bettencourt, A.P. Electro-oxidation of d-mannose on platinum, gold and nickel electrodes in aqueous medium. *J. Electroanal. Chem.* **2007**, *610*, 154–162. [CrossRef]

29. Gabriel, K.R. Biplot graphic display of matrices with application to principal component analysis. *Biometrika* **1971**, *58*, 453–467. [CrossRef]

30. Lobato, J.; González del Campo, A.; Fernández, F.J.; Cañizares, P.; Rodrigo, M.A. Lagooning microbial fuel cells: A first approach by coupling electricity-producing microorganisms and algae. *Appl. Energy* **2013**, *110*, 220–226. [CrossRef]

31. Elgrishi, N.; Rountree, K.J.; McCarthy, B.D.; Rountree, E.S.; Eisenhart, T.T.; Dempsey, J.L. A Practical Beginner's Guide to Cyclic Voltammetry. *J. Chem. Educ.* **2018**, *95*, 197–206. [CrossRef]

32. Ryckelynck, N.; Stecher, H.A.; Reimers, C.E. Understanding the Anodic Mechanism of a Seafloor Fuel Cell: Interactions between Geochemistry and Microbial Activity. *Biogeochemistry* **2005**, *76*, 113–139. [CrossRef]

33. Mitov, M.; Bardarov, I.; Mandjukov, P.; Hubenova, Y. Chemometrical assessment of the electrical parameters obtained by long-term operating freshwater sediment microbial fuel cells. *Bioelectrochemistry* **2015**, *106*, 105–114. [CrossRef] [PubMed]

34. Fan, Y.; Sharbrough, E.; Liu, H. Quantification of the Internal Resistance Distribution of Microbial Fuel Cells. *Environ. Sci. Technol.* **2008**, *42*, 8101–8107. [CrossRef] [PubMed]

35. Song, T.-S.; Yan, Z.-S.; Zhao, Z.-W.; Jiang, H.-L. Construction and operation of freshwater sediment microbial fuel cell for electricity generation. *Bioprocess Biosyst. Eng.* **2011**, *34*, 621–627. [CrossRef] [PubMed]

36. Call, D.F.; Merrill, M.D.; Logan, B.E. High surface area stainless steel brushes as cathodes in microbial electrolysis cells. *Environ. Sci. Technol.* **2009**, *43*, 2179–2183. [CrossRef]

37. Logan, B.E.; Hamelers, B.; Rozendal, R.; Schröder, U.; Keller, J.; Freguia, S.; Aelterman, P.; Verstraete, W.; Rabaey, K. Microbial Fuel Cells: Methodology and Technology. *Environ. Sci. Technol.* **2006**, *40*, 5181–5192. [CrossRef]

38. Pfeffer, C.; Larsen, S.; Song, J.; Dong, M.; Besenbacher, F.; Meyer, R.L.; Kjeldsen, K.U.; Schreiber, L.; Gorby, Y.A.; El-Naggar, M.Y.; et al. Filamentous bacteria transport electrons over centimetre distances. *Nature* **2012**, *491*, 218–221. [CrossRef] [PubMed]

39. Nielsen, L.P.; Risgaard-Petersen, N. Rethinking Sediment Biogeochemistry after the Discovery of Electric Currents. *Ann. Rev. Mar. Sci.* **2015**, *7*, 425–442. [CrossRef]

40. Risgaard-Petersen, N.; Kristiansen, M.; Frederiksen, R.B.; Dittmer, A.L.; Bjerg, J.T.; Trojan, D.; Schreiber, L.; Damgaard, L.R.; Schramm, A.; Nielsen, L.P. Cable Bacteria in Freshwater Sediments. *Appl. Environ. Microbiol.* **2015**, *81*, 6003–6011. [CrossRef]

41. Ribeiro, D.C.; Martins, G.; Nogueira, R.; Brito, A.G. Mineral cycling and pH gradient related with biological activity under transient anoxic-oxic conditions: Effect on P mobility in volcanic lake sediments. *Environ. Sci. Technol.* **2014**, *48*, 9205–9210. [CrossRef] [PubMed]

42. Marzocchi, U.; Trojan, D.; Larsen, S.; Louise Meyer, R.; Peter Revsbech, N.; Schramm, A.; Peter Nielsen, L.; Risgaard-Petersen, N. Electric coupling between distant nitrate reduction and sulfide oxidation in marine sediment. *ISME J.* **2014**, *8*, 1682–1690. [CrossRef] [PubMed]

43. Asensio, Y.; Montes, I.B.; Fernandez-Marchante, C.M.; Lobato, J.; Cañizares, P.; Rodrigo, M.A. Selection of cheap electrodes for two-compartment microbial fuel cells. *J. Electroanal. Chem.* **2017**, *785*, 235–240. [CrossRef]

44. Sacco, N.J.; Figuerola, E.L.M.; Pataccini, G.; Bonetto, M.C.; Erijman, L.; Cortón, E. Performance of planar and cylindrical carbon electrodes at sedimentary microbial fuel cells. *Bioresour. Technol.* **2012**, *126*, 328–335. [CrossRef] [PubMed]

45. Brito, A.G.; Melo, L.F. Mass transfer coefficients within anaerobic biofilms: Effects of external liquid velocity. *Water Res.* **1999**, *33*, 3673–3678. [CrossRef]

46. Li, Y.; Williams, I.; Xu, Z.; Li, B.; Li, B. Energy-positive nitrogen removal using the integrated short-cut nitrification and autotrophic denitrification microbial fuel cells (MFCs). *Appl. Energy* **2016**, *163*, 352–360. [CrossRef]

47. Hong, S.W.; Chang, I.S.; Choi, Y.S.; Kim, B.H.; Chung, T.H. Responses from freshwater sediment during electricity generation using microbial fuel cells. *Bioprocess Biosyst. Eng.* **2009**, *32*, 389–395. [CrossRef] [PubMed]

48. Martins, G.; Ribeiro, D.C.; Pacheco, D.; Cruz, J.V.; Cunha, R.; Gonçalves, V.; Nogueira, R.; Brito, A.G. Prospective scenarios for water quality and ecological status in Lake Sete Cidades (Portugal): The integration of mathematical modelling in decision processes. *Appl. Geochem.* **2008**, *23*, 2171–2181. [CrossRef]

49. Daghio, M.; Aulenta, F.; Vaiopoulou, E.; Franzetti, A.; Arends, J.B.A.; Sherry, A.; Suárez-Suárez, A.; Head, I.M.; Bestetti, G.; Rabaey, K. Electrobioremediation of oil spills. *Water Res.* **2017**, *114*, 351–370. [CrossRef] [PubMed]

50. Bellagamba, M.; Cruz Viggi, C.; Ademollo, N.; Rossetti, S.; Aulenta, F. Electrolysis-driven bioremediation of crude oil-contaminated marine sediments. *New Biotechnol.* **2017**, *38*, 84–90. [CrossRef] [PubMed]